ACS APPLIED MATERIALS & INTERFACES

Research Article

www.acsami.org

An Approach for an Advanced Anode Interfacial Layer with Electron-Blocking Ability to Achieve High-Efficiency Organic Photovoltaics

Jun-Seok Yeo,[†] Jin-Mun Yun,[‡] Minji Kang,[†] Dongyoon Khim,[†] Seung-Hoon Lee,[†] Seok-Soon Kim,[§] Seok-In Na,*[,∥] and Dong-Yu Kim*[,†]

[†]Heeger Center for Advanced Materials (HCAM), School of Materials Science and Engineering, Gwangju Institute of Science and Technology, Gwangju, 500-712, Republic of Korea

[‡]Radiation Research Division for Industry and Environment, Korea Atomic Energy Research Institute (KAERI), 29 Geumgu-gil, Jeongeup-si, Jeollabuk-do, 580-185, Republic of Korea

[§]School of Materials Science and Chemical Engineering, Kunsan National University, Kunsan, Jeollabuk-do, 753-701, Republic of Korea

[∥]Professional Graduate School of Flexible and Printable Electronics, Polymer Materials Fusion Research Center, Chonbuk National University, Jeonju-si, Jeollabuk-do, 561-756, Republic of Korea

Supporting Information

ABSTRACT: The interfacial properties of PEDOT:PSS, pristine r-GO, and r-GO with sulfonic acid (SR-GO) in organic photovoltaic are investigated to elucidate electron-blocking property of PEDOT:PSS anode interfacial layer (AIL), and to explore the possibility of r-GO as electron-blocking layers. The SR-GO results in an optimized power conversion efficiency of 7.54% for PTB7-th:$PC_{71}BM$ and 5.64% for P3HT:$IC_{61}BA$ systems. By combining analyses of capacitance−voltage and photovoltaic-parameters dependence on light intensity, it is found that recombination process at SR-GO/active film is minimized. In contrast, the devices using r-GO without sulfonic acid show trap-assisted recombination. The enhanced electron-blocking properties in PEDOT:PSS and SR-GO AILs can be attributed to surface dipoles at AIL/acceptor. Thus, for electron-blocking, the AIL/acceptor interface should be importantly considered in OPVs. Also, by simply introducing sulfonic acid unit on r-GO, excellent contact selectivity can be realized in OPVs.

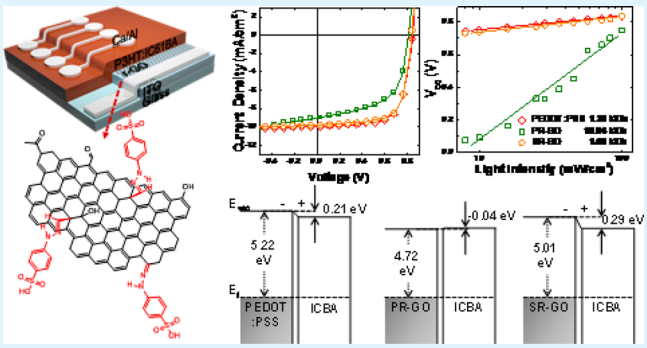

KEYWORDS: *organic solar cells, graphene oxide, electron-blocking, interfacial layer, charge recombination*

1. INTRODUCTION

In organic photovoltaics (OPVs) adopting the inevitable concept of bulk-heterojunction (BHJ), tremendous efforts have been devoted to enhancing power conversion efficiency (PCE) via the development of promising light-absorbing materials, device optimization with different structures, and the application of innovative processing techniques.[1−7] Also, the advancements of OPV performances have been accomplished by interface engineering between active layer and electrodes.[8,9] For interface modulation, a diverse range of materials has been developed to date, and, in particular, with regard to the anode side, numerous materials have been proven effective as interface modifiers. This includes the conventional poly(3,4-ethylenedioxythiophene):poly(styrenesulfonate) (PEDOT:PSS), metal oxides,[10,11] and small molecules.[12] In addition, the graphene oxide (GO) has been recently demonstrated as a viable anode interfacial layer (AIL) due to excellent and adjustable electrical properties, simple solution-processability, and efficient passivation-property for long-term device stability.[13−15] Using this route, the successful demonstration of reduced graphene oxide (r-GO) as an AIL in OPV was also reported with excellent efficiency and device stability superior to those obtained in conventional devices with a PEDOT:PSS AIL.[16] Furthermore, by tailoring electrical properties of r-GO using sulfonic acid functionality ($-SO_3H$), the extended capability of r-GO AILs to be operated under various polymer donor systems regardless of the highest occupied molecular orbital (HOMO) level of polymers was achieved,[17] which was mainly attributed to energy level matching for ohmic contacts resulting in favorable charge-extraction.

Besides cascade-energy-level adjustment for efficient charge-extraction, the secure and efficient charge-transport of individual charge carriers (electrons and holes) with a

Received: June 20, 2014
Accepted: October 24, 2014
Published: October 24, 2014

minimized recombination loss is also an essential factor for achieving a desirable device performance.[8,18] For BHJ architectures, however, interpenetrating networks of donor and acceptor components typically suffer from undesirable electrical contacts such as anode/acceptor and cathode/donor, which results in charge recombination events to induce the degradation in the overall photovoltaic characteristics.[8,9] Therefore, in addition to adequate energy alignment between the electrodes and the BHJ layers for ohmic contact, the contact should be selective to reduce contact recombination at the appropriate electrode. In addition, although the PEDOT:PSS is commonly used as AILs and some reports have shown electron-blocking properties including blocking of exciton quenching,[19−24] which are probably due to the surface-enriched PSS component at the surface of PEDOT:PSS film,[24] there is still some need for the more actual and detailed reasons of the electron-blocking contribution from PEDOT:PSS AILs. Moreover, even though the aforementioned r-GO promises to be an attractive alternative to PEDOT:PSS AILs, the issues surrounding the charge-blocking properties of r-GO AILs in OPV devices have been not addressed in the literature. For further exploring the potential of r-GO AILs for general use in OPVs, the investigation on their charge-blocking properties should be carried out as an equally critical factor to hole-transport via ohmic formations.

In this article, we introduce an effective approach for a generally applicable AIL, achieving not only a favorable hole-transport property but also a remarkable electron-blocking ability in BHJ-OPVs. As the anode interfacial modifier, conventional PEDOT:PSS, pristine reduced graphene oxide (PR-GO), and sulfonic acid-grafted reduced graphene oxide (SR-GO) were used where SR-GO was recently developed and showed the successful AIL performance in OPVs via favorable energy level alignment for ohmic contacts with diverse donor systems.[17] To understand the mechanism of the electron-blocking ability from PEDOT:PSS AIL and to investigate whether the r-GO can be an electron-blocking layer or not, we selected these well-known r-GO AILs because the main structures of PR-GO and SR-GO are identically based on reduced graphene oxides, but SR-GO containing $-SO_3H$ units that are substantial portions of PEDOT:PSS is expected to inherit the anode interfacial properties of PEDOT:PSS. We first applied these various AIL systems in BHJ-OPVs employing PTB7-th:$PC_{71}BM$ ([6,6]-phenyl-C_{71}-butyric acid methyl ester), where the PTB7-th is the PTB7 derivative showing the extended absorption band and higher HOMO level as compared to the original PTB7,[25] and its chemical structure is provided in Supporting Information Figure S1. For the PTB7-th:$PC_{71}BM$ devices, we obtained high photovoltaic characteristics with no significant differences in PCE values among different AIL systems (7.58% for PEDOT:PSS, 6.89% for PR-GO, and 7.54% for SR-GO). However, when the donor:acceptor pair was changed to poly(3-hexylthiophene):indene-C60 bisadduct (P3HT:$IC_{61}BA$), we found that PCE of OPVs with SR-GO exhibited a highly improved value of 5.64% as compared to the PR-GO-based cell efficiency of 3.85%, resulting mainly from a more effectively blocked carrier recombination at the interface between SR-GO AIL and BHJ layers. To arrive at the conclusion related to the electron-blocking, the detailed identification and characterization of the interface energetics including recombination kinetics between r-GO AILs and BHJ layer were performed using the measurements of capacitance−voltage ($C-V$), light intensity dependence in the current density−voltage ($J-V$), and ultraviolet photoemission spectroscopy (UPS). We finally found that the formation of an interfacial dipole between SR-GO and $IC_{61}BA$ layers caused by sulfonic acid functionality can suppress undesirable electron leakage and recombination, thereby achieving high-performing BHJ devices.

2. EXPERIMENTAL DETAILS

Synthesis of Reduced Graphene Oxides (r-GO). At the first step, the graphene oxide (GO) was prepared according to previous reports, and the resultant GO was dispersed in deionized water at a concentration of 3 mg mL^{-1} for the chemical reduction process. To synthesize PR-GO, 5 g of *p*-toluenesulfonyl hydrazide as a reductant was added into the GO aqueous solution (3 mg mL^{-1}, 30 mL), and then the mixed solution was heated at 60 °C with stirring for 24 h. After the completion of the reduction process, the filtration of floating suspension was performed, and the remaining reductant was removed by sequentially washing with water and dimethylformamide. A homogeneous PR-GO dispersion was achieved by dispersing PR-GO flakes in dimethylformamide with a concentration of 0.6 mg mL^{-1}. In addition, for SR-GO synthesis, *p*-hydrazinobenzenesulfonic acid hemihydrate (5 g) was added into the GO aqueous solution (3 mg mL^{-1}, 30 mL), and then the mixture solution was stirred at 60 °C heating for 24 h. After that, for precipitation of the SR-GO, a small amount of sodium chloride was added into the mixture solution. The floating SR-GO was centrifuged at 10 000 rpm for 10 min, and then washed with methanol at least three times. The produced SR-GO was redispersed in deionized water with a concentration of ∼0.6 mg mL^{-1}.

Sample Characterizations. The measurements of X-ray photoemission spectroscopy (XPS) and UPS (AXIS NOVA, Kratos) were carried out using a monochromatized Al Kα for XPS, and the He I ($h\nu$ = 21.2 eV) excitation source with energy resolution of 0.1 eV for UPS under a pressure of 5×10^{-8} Torr. The Fermi energy reference for UPS analysis was determined using a cleaned gold surface. The r-GO thickness of reduced graphene oxides was measured using an atomic force microscope (Dimension 3100, Veeco) with tapping mode as shown in Supporting Information Figure S2. The electrical sheet resistance and conductivity were measured with a four-point-probe system (FPP RS8, Dasol Eng.).

OPV Fabrication and Characterization. The cleaned ITO/glass substrates were treated with UV/O_3 for 15 min. The r-GO solutions and PEDOT:PSS (Clevios P VP AI 4083, Heraeus) were deposited by spin coating at 5000 rpm for 40 s onto the prepared substrates, and then all substrates were heated at 120 °C during 10 min. To fabricate BHJ photoactive films, P3HT (4002-EE, Rieke Metals), PTB7-th (1-material), $PC_{61}BM$ (Nano-C), $PC_{71}BM$ (Nano-C), and $IC_{61}BA$ (1-material) were used without further purification. A BHJ active solution composed of either P3HT:$PC_{61}BM$ or P3HT:$IC_{61}BA$ was spin coated onto the substrate at 700 rpm for 60 s, and then a slow evaporation of active-film was carried out by keeping the film in a capped-glass jar for 2 h, followed by thermal treatments (150 °C for 10 min). For high-performance OPVs, a chlorobenzene solution (1 mL) consisting of a mixture of PTB7-th:$PC_{71}BM$ (10 mg:15 mg) and 1,8-diiodooctane (3 vol %) was spin-cast at 2000 rpm for 40 s onto a prepared substrate. Finally, top electrodes composed of Ca (20 nm)/Al (80 nm) were deposited through a shadow mask (active area: 4.64 mm^2) using a thermal evaporator in a vacuum of a pressure of 10^{-6} Torr. The current density−voltage ($J-V$) plots were recorded using a Keithley 2400 instrument under 100 mW cm^{-2} illumination with simulated AM 1.5 G condition and using the standard Si solar cell certified by the International System of Units (SI) (SRC 1000 TC KG5 N, VLSI Standards, Inc.). The direction of the voltage scan was forward bias (1.0 V) to reverse bias (−1.0 V), and the step voltage was fixed at 20 mV. The EQE and IQE spectra were measured via a Quantum Efficiency Measurement System (IQE-200, Oriel). The J_{SC} values calculated from EQE spectra were within 3% error as compared to the corresponding J_{SC} measured in $J-V$ curves. The capacitance−voltage ($C-V$) characteristics were measured under dark condition, and at a fixed frequency of 10 kHz using Agilent 4284A precision LCR meter

with Keithley 4200-SCS setup. AC oscillating voltage was as low as 20 mV for the linearity of the response. The sample preparation for $C-V$ measurement was the same as that used for $J-V$ measurements.

OFET Fabrication and Characterization. The top-gate and top-contact (TG/TC) OFETs were fabricated on glass substrates with patterned PEDOT:PSS, PR-GO, and SR-GO layers. After the deposition of patterned AIL films, very thin blend films (10 nm) were spin-coated on prepared substrates, and then 50 nm thick gold contact for source and drain electrodes were fabricated with a shadow mask (W = 1000 μm, L = 50 μm) using a thermal evaporator under a vapor pressure of ~10^{-6} Torr. The fluoro-polymer poly-(perfluorobutenylvinylether) (CYTOPTM, CTL-809M) and a per-fluorocarbon-containing solvent (CT-Solv. 180) from Asahi Glass were mixed with 3:1 volume ratio for the gate dielectric layer. After spin-coating the dielectric layer on the prepared films, the device fabrication was completed by evaporation of Al for gate electrode with thickness of 50 nm. The resultant OFET electrical performances were obtained with Keithley 4200-SCS in a N_2-filled glovebox.

3. RESULTS AND DISCUSSION

We synthesized PR-GO and SR-GO according to procedures outlined in a previous report[17] using either *p*-toluenesulfonyl hydrazide (PR-GO) or *p*-hydrazinobenzenesulfonic acid hemi-hydrate (SR-GO) as a reductant, which resulted in different surface functionalizations for GO nanosheets with or without $-SO_3H$. Additional control experiments using PEDOT:PSS as the most popular AILs in OPVs were also carried out to systematically compare the surface chemistries, electrical properties, and interface energetics as an electron-blocking layer with the r-GO systems. First, for insight into the surface chemical composition of PEDOT:PSS, PR-GO, and SR-GO thin films, we conducted analysis of the surface chemistries using XPS, and Figure 1 shows the corresponding XPS profiles.

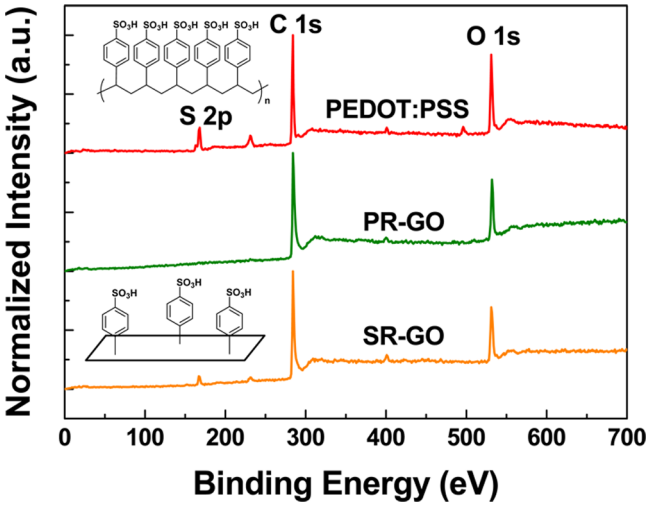

Figure 1. XPS survey profiles of different anode interfacial materials.

The high relative peak-intensity of C 1s to O 1s in two kinds of r-GOs reflected the high degree of reduction from GO containing carboxylic, epoxy, carbonyl, and hydroxyl units to a nonoxidized aromatic network of a graphene basal plane,[26] thus leading to high electrical conductivity of r-GO samples. Here, the conductivity values of the PR-GO and the SR-GO were about 1 and 3 S cm^{-1}, respectively, which are both significantly above the conductivity of commonly used PEDOT:PSS (~10^{-3} S cm^{-1}), and these high conductivities of AILs could improve the series resistance of the resultant device, thereby enhancing other photovoltaic parameters such as short-circuit current density (J_{SC}) and fill factor (FF).[8,9] More importantly, the peaks at a binding energy of approximately 168 eV in the S (sulfur) 2p spectrum were clearly observed in PEDOT:PSS and SR-GO samples, which corresponded to the sulfur atoms in the $-SO_3H$ units comprising PSS chains of PEDOT:PSS and surface functional groups on the basal plane of SR-GO, respectively.[17,19] The intensities of the sulfonic acid units in SR-GO were less than those of PEDOT:PSS, indicating a higher degree of the sulfonic acid presence on the PEDOT:PSS surface than that on the surface of SR-GO. On the other hand, as expected, the peak associated with sulfonic acid was not seen in the S p2 spectrum of a PR-GO sample.

To directly access the role of $-SO_3H$ functionality on the PEDOT:PSS and r-GO surfaces in device performance, we fabricated BHJ-OPVs comprised of PTB7-th:$PC_{71}BM$ blends using different AILs such as PEDOT:PSS (~25 nm), PR-GO (~2 nm), and SR-GO (~2 nm). The $J-V$ characteristics for representative devices are shown in Figure 2, the average values with standard deviations were summarized in Table 1, and they were extracted from characterization for over 10 devices. In the devices comprising P3HT:$PC_{61}BM$ (1-(3-methoxycarbonyl)-propyl-1-phenyl-(6,6)C_{61}) BHJ as depicted in the Supporting Information (Figure S3), the resultant OPVs showed highly optimized cell performances in both types of r-GO AIL systems, giving rise to comparable PCE values for PEDOT:PSS-based devices, which could be originated from well-established ohmic contact at PR-GO/P3HT, and SR-GO/P3HT interfaces like PEDOT:PSS/P3HT interface. For the active layer of PTB7-th:$PC_{71}BM$, the BHJ devices were confirmed to offer excellent cell-performance in both cases of PR-GO and SR-GO, where the PCE for SR-GO was slightly enhanced from PR-GO cells. The average open-circuit voltage (V_{OC}), J_{SC}, FF, and PCE of devices based on PR-GO and SR-GO showed 0.76 and 0.77 V, 13.18 and 13.92 mA cm^{-2}, 69.2% and 70.4%, and 6.89% and 7.54%, respectively. These performances closely approached the OPVs employing PEDOT:PSS AIL, yielding the PCE of 7.58%. Note that a change of donor components used in BHJ systems from P3HT to PTB7-th did not induce a significant influence of AIL types on device performance.

Interestingly, however, when P3HT:$IC_{61}BA$ BHJ was incorporated into OPVs as an active layer (i.e., the acceptor component was changed from PCBM to ICBA) where $IC_{61}BA$ is a promising fullerene derivative with a higher-lying lowest unoccupied electron orbitals (LUMO) level for improvement in the open-circuit voltage,[27] completely different behaviors were observed in two kinds of r-GO AILs. As shown in Figure 3a, the photovoltaic characteristics of SR-GO incorporated cell exhibited an average V_{OC} of 0.83 V, an average J_{SC} of 9.66 mA cm^{-2}, an average FF of 70.3%, and an average PCE of 5.64%. Those values were similar to the performance of an optimized OPV with PEDOT:PSS film as shown in Table 2. However, when the PR-GO film was employed as an AIL, the devices showed an inferior performance: a V_{OC} of 0.79 V; a J_{SC} of 8.92 mA cm^{-2}; a FF of 54.5%; and a PCE of 3.85%. Similar trends were found in the diode characteristics of the same devices under dark condition as shown in Figure 3b: highly unstable current along with reverse bias for a PR-GO cell, and a much reduced leakage current for the device with a SR-GO AIL. It can be expressed in terms of the numerical resistances calculated from the dark $J-V$ plots: a series resistance of 2.75 Ω cm^2 for PR-GO, and 2.70 Ω cm^2 for SR-GO; and a shunt

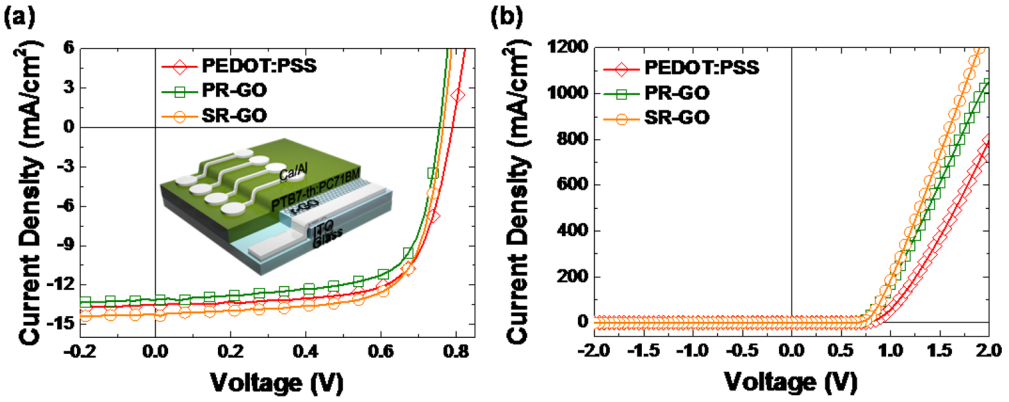

Figure 2. Representative $J-V$ plots of devices based on different AILs with PTB7-th:$PC_{71}BM$ BHJ (a) under AM 1.5 G illumination at 100 mW cm^{-2}, and (b) under dark condition.

Table 1. Photovoltaic Characteristics with Average Values for PTB7-th:$PC_{71}BM$ BHJ Cells Comprising Different AILs

AIL	V_{OC} (V)	J_{SC} (mA cm^{-2})	FF (%)	PCE (%)
PEDOT:PSS	0.79 ± 0.01	13.68 ± 0.18	70.1 ± 0.6	7.58 ± 0.18
PR-GO	0.76 ± 0.01	13.18 ± 0.09	69.2 ± 0.6	6.89 ± 0.17
SR-GO	0.77 ± 0.01	13.92 ± 0.41	70.4 ± 0.5	7.54 ± 0.06

resistance of 0.126 kΩ cm^2 for PR-GO, and 53.6 kΩ cm^2 for SR-GO, respectively. An unexpected but great dependence of electron acceptor types on device performances is observed for r-GO AIL systems, strongly suggesting that the interface of AIL/acceptor in BHJ has a significant influence on the OPV performances in addition to AIL/donor interfaces. Considering that the two types of r-GOs present a favorable energetic alignment with P3HT for ohmicity and comparable series resistance, the capability of electron-blocking at the r-GO/BHJ (r-GO/acceptor to be exact) interface could lead mainly to a deviation in the overall efficiency of devices with P3HT:$IC_{61}BA$ BHJ between PR-GO and SR-GO systems. The results obtained from the $J-V$ characteristics were well consistent with external quantum efficiency (EQE) and internal quantum efficiency (IQE) as shown in Figure 3c. There are negligible EQE and IQE intensity deviations in PEDOT:PSS- and SR-GO-based OPVs, indicating that charge-extraction ability of SR-GO cells employing P3HT:$IC_{61}BA$ blends is comparable to that of optimized PEDOT:PSS device. However, the PR-GO cells failed to approach the quantum efficiency spectra for those of PEDOT:PSS, and, in particular, the IQE spectrum of the PR-GO cell showed a lower value in overall range of wavelength relative to the reference PEDOT:PSS spectrum. Considering that the IQE is highly linked to exciton diffusion, dissociation, and charge-extraction, where exciton diffusion and dissociation are strongly related to the identically used active morphology,[28] the low value of IQE for PR-GO devices could result from a relatively poor charge-extraction efficiency, which could be due to activated recombination within PR-GO devices before extraction of photogenerated charge carriers.

To further examine the effects of AILs on the interface electronic states in the BHJ-OPV devices, the capacitance of devices used in $J-V$ measurements was measured as a function of applied bias under dark condition via Mott−Schottky (MS) analysis. The capacitance induced by the depletion region, as expressed by the equation $C^{-2} = 2(V_{bi} - V)/(q\varepsilon N)$, dominates the overall capacitance before the flat band conditions (built-in voltage $V_{bi} = V$),[29,30] where V is the applied bias, q corresponds to the elementary charge, ε is the dielectric constant, and N is the impurity concentration. As depicted in Figure 4a, a higher depletion capacitance was observed in the PR-GO-based diode as compared to the PEDOT:PSS and SR-GO devices. The N values obtained from the linear relationship in $C^{-2}-V$ for the applied voltage range between low forward bias and V_{bi} as presented in Figure 4b were 5.75×10^{15}, 1.28×10^{16}, and 6.00×10^{15} cm^{-3} for PEDOT:PSS, PR-GO, and SR-GO, respectively. Also, the V_{bi} was derived from MS plot of C^{-2} by extrapolating its linear portion to the voltage axis as follows: 0.76, 0.73, and 0.76 V for PEDOT:PSS, PR-GO, and SR-GO, respectively. The higher capacitance at approaching V_{bi} and higher impurity concentration in the case of PR-GO system measured under dark condition support a more facilitated charge recombination in an illuminated state.[31,32] Meanwhile, as expected, the injection barrier at the metal contact/BHJ interface was consistently minimized for all devices regardless of AIL types, as evidenced by the sufficient built-in voltage, exponential increase and nonsaturated values of the capacitance, along with the high forward voltage shown in Figure 4a for all types of devices with different AILs.[30,33]

For insight into the influence of capacitance and impurity concentration as measured under dark conditions on photovoltaic parameters, the dependence of V_{OC} and J_{SC} on light intensity (P_{light}) was carefully probed and analyzed as shown in Figure 4c and Supporting Information Figure S4. In the open-circuit state, no photogenerated carriers are extracted to the outside of the cells because all photocharge carriers are recombined within the devices, which provides qualitative information on the recombination kinetics of BHJ-OPVs.[34−36] In general, the optimized OPVs comprising polymer:fullerene BHJ dominantly obey the bimolecular recombination (Langevin recombination) mechanism, and for bimolecular recombination, the V_{OC} can be given simply by $V_{OC} = (kT/q) \times \ln(P_{light}) + \text{constant}$, and thus the slope ($S$) of V_{OC} versus $\ln(P_{light})$ will be equal to kT/q.[35,36] As shown in Figure 4c, the dependence of V_{OC} on light intensity was varied according to the devices with different AIL types: S = 1.38, 10.94, and 1.49 kT/q for PEDOT:PSS, PR-GO, and SR-GO in P3HT:$IC_{61}BA$ BHJ systems, while the S obtained from P3HT:$PC_{61}BM$ BHJ

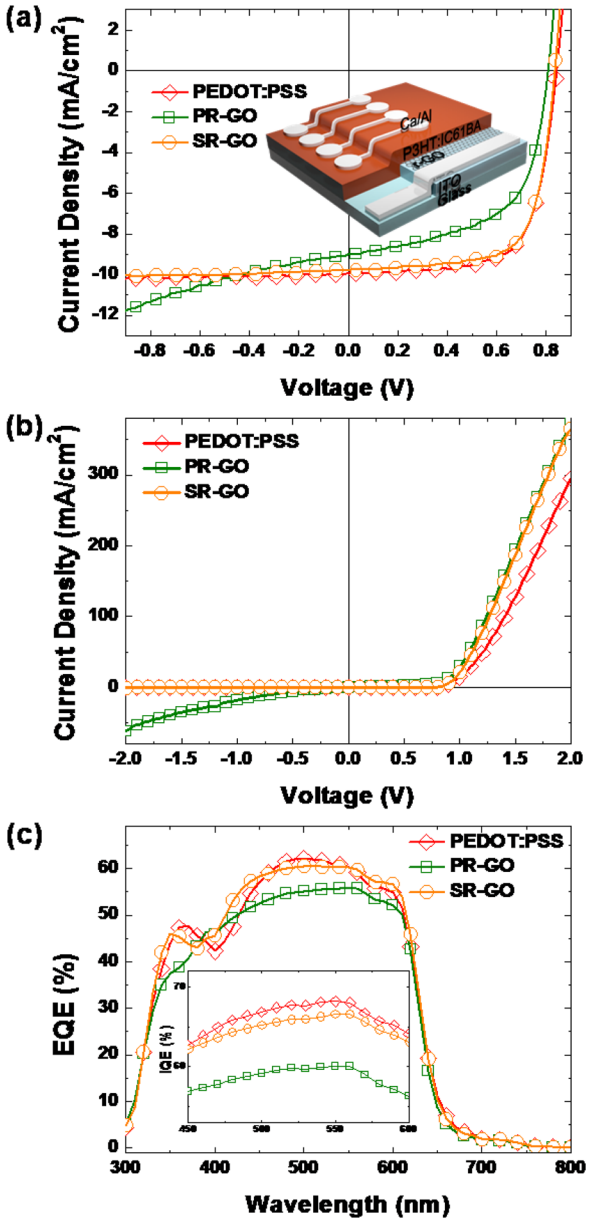

Figure 3. Representative $J-V$ curves for P3HT:$IC_{61}BA$ BHJ (a) under AM 1.5G illumination at 100 mW cm^{-2} and (b) under dark condition. (c) External quantum efficiency (EQE) spectra of devices with different AILs. The inset shows internal quantum efficiency spectra of corresponding devices.

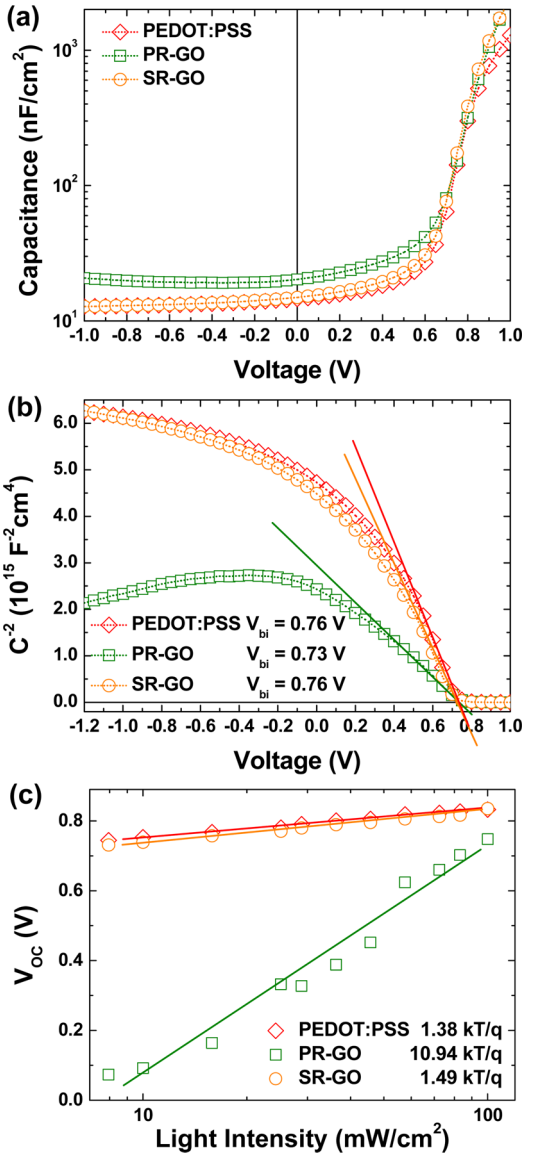

Figure 4. (a) The capacitance as a function of applied voltage at a 10 kHz frequency for diodes used in $J-V$ measurements. (b) Mott–Schottky plots that exhibit a straight line providing V_{bi} and N (assuming ε (relative dielectric constant) = 3 for P3HT:$IC_{61}BA$ blends). (c) The dependence of the open-circuit voltage on light intensity of corresponding devices with linear fitting to measured data in a semilogarithmic scale.

systems showed comparable values regardless of AIL types as provided in Supporting Information Figure S5. Taking into account $S \approx kT/q$ for PEDOT:PSS and SR-GO, the bimolecular recombination process was obviously dominant in these systems, which indicates that the presence of PEDOT:PSS/$IC_{61}BA$ and SR-GO/$IC_{61}BA$ in BHJ devices rarely promotes recombination strength. Unlike the case of PEDOT:PSS and SR-GO, a much steeper V_{OC} dependence on the P_{light} for PR-GO was observed with high S values, indicating that the trap-assisted recombination (Shockley–Read–Hall recombination) mainly determined the recombination process for PR-GO devices, which assumes that the increased impurity concentration measured in C–V analysis led to a significant degree of activated charge recombination events, probably due to the presence of PR-GO/$IC_{61}BA$ interfaces. This result implies that the PR-GO AIL in a P3HT:$IC_{61}BA$ BHJ system

Table 2. Photovoltaic Parameters with Average Values for P3HT:$IC_{61}BA$ BHJ Devices Based on Different AILs

AIL	V_{OC} (V)	J_{SC} (mA cm^{-2})	FF (%)	PCE (%)
PEDOT:PSS	0.84 ± 0.01	9.75 ± 0.01	69.2 ± 0.2	5.68 ± 0.07
PR-GO	0.79 ± 0.01	8.92 ± 0.08	54.5 ± 0.1	3.85 ± 0.06
SR-GO	0.83 ± 0.01	9.66 ± 0.08	70.3 ± 0.3	5.64 ± 0.03

dx.doi.org/10.1021/am503989u | ACS Appl. Mater. Interfaces 2014, 6, 19613–19620

could not passivate the local shunts at the PR-GO/$IC_{61}BA$ interfaces, which acted as an electrical leakage path, and thereby failed to achieve an efficient charge-blocking capability, leading to simultaneous degradations in V_{OC}, J_{SC}, and FF. Consequently, the significantly reduced recombination strength could be considered as a major contribution to the enhanced device efficiency of PEDOT:PSS and SR-GO. On the contrary, PR-GO devices failed to achieve an efficient charge-blocking capability due to increased strength of recombination, which could be due to the difference in the interfacial properties of AIL/$IC_{61}BA$ junctions among PEDOT:PSS, PR-GO, and SR-GO systems.[37−39]

To understand the electron-blocking origins of PEDOT:PSS and the different behaviors of the two kinds of r-GOs, we used the UPS to study the interface energetics between AILs and $IC_{61}BA$, because the interfacial properties of AIL/$IC_{61}BA$ would play a critical role in determining the recombination strength. Figure 5a illustrates the secondary electron cutoff spectra of a thin $IC_{61}BA$ layer (~3 nm) on PEDOT:PSS, PR-GO, and SR-GO layers, the corresponding schematic energy diagrams derived from the UPS results are depicted in Figure 5b, and the UPS spectra with regard to AIL/$PC_{61}BM$ interfaces are also presented in Supporting Information Figure S6. As the shift of the electron cutoff onset shows, there were vacuum level (E_{vac}) shifts at the PEDOT:PSS/$IC_{61}BA$ and SR-GO/$IC_{61}BA$ interfaces, yielding a surface dipole of 0.21 and 0.29 eV for PEDOT:PSS and SR-GO, respectively.[40] The formation of the dipole at the interface enhanced the electron-blocking properties,[11] which could be due to the surface species, that is, $-SO_3H$, in both cases of PEDOT:PSS and SR-GO. Furthermore, because the sulfonic acid unit could act as a proton source via an electrochemical reaction with subsequent organic layer,[17,20] the enhanced hole-selective behavior could also have arisen from the p-doped adjacent BHJ layer,[41] which can be confirmed by UPS spectra around the Fermi level and p-channel field-effect transistor characteristics of the BHJ films as presented in Supporting Information Figures S7 and S8. As is evident in Figure 5, and Supporting Information Figures S7 and S8, even if the degree of $-SO_3H$ presence on the SR-GO surface, as confirmed in XPS analysis, was lower than that in the PEDOT:PSS films, it was sufficient to form a surface dipole with the doping of sequential organic layer for the accomplishment of an efficient anode-selectivity. In contrast, in the case of PR-GO/$IC_{61}BA$, a negligible energy offset appeared, which implies no existence of surface dipole at the PR-GO/$IC_{61}BA$ interface and no doping phenomena with subsequent $IC_{61}BA$ layer as shown in Supporting Information Figures S7 and S8. Thus, all consequences of aforementioned investigation provide that the existence of $-SO_3H$ units on the PEDOT:PSS surface is attributed to an enhanced anode contact-selectivity via the formation of a local interfacial dipole with acceptor components. Furthermore, under r-GO circumstances, although inherent properties of r-GO as metals lead to a poor capability of electron-blocking at the anode contacts,[15] via surface functionalization with $-SO_3H$ units, the SR-GO functions as an effective electron-blocking layer similar to PEDOT:PSS AILs.

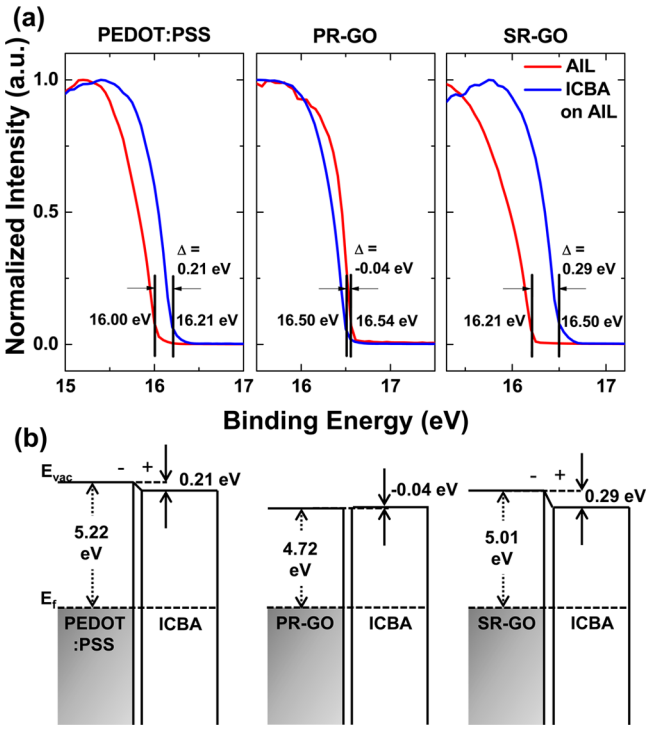

Figure 5. (a) UPS spectra onset in the secondary electron cutoff region for thin $IC_{61}BA$ films on PEDOT:PSS, PR-GO, and SR-GO. (b) Schematic illustration of resultant energy level diagram showing interfacial dipoles.

4. CONCLUSIONS

We investigated the electron-blocking properties of the well-known PEDOT:PSS, r-GO, and r-GO functionalized with $-SO_3H$ similar to PEDOT:PSS in OPVs based on two different BHJ systems (PTB7-th:$PC_{71}BM$ and P3HT:$IC_{61}BA$) to gain a better understanding into the origins of electron-blocking properties of a PEDOT:PSS AIL. We also explored the possibility of using r-GO as an electron-blocking layer. The $-SO_3H$ functionalized SR-GO resulted in highly efficient PCE of 7.54% for PTB7-th:$PC_{71}BM$ and 5.64% for P3HT:$IC_{61}BA$ BHJ, which were comparable to those obtained in devices with PEDOT:PSS AIL and obviously benefited from an increase in the degree of electron-blocking capability relative to pristine r-GO systems, especially for the P3HT:$IC_{61}BA$ BHJ case. $C-V$ characteristics and photovoltaic-parameter dependence on light intensity revealed that the recombination process at SR-GO/BHJ was minimized, while there was a trap-assisted recombination phenomenon in PR-GO devices, which adversely affected electron-blocking at AIL/BHJ interface. We attributed this enhanced electron-blocking phenomena in PEDOT:PSS and SR-GO systems to the formation of surface dipoles between AIL and $IC_{61}BA$ layers due to sulfonic acid functionality, which was not observed in PR-GO systems. Thus, we concluded that the primary reason for a deviation in the overall efficiency of BHJ-OPVs among PEDOT:PSS, PR-GO, and SR-GO systems could be due to the interface characteristics of AIL/acceptor junctions in terms of electron-blocking, and it should be considered as an equally important aspect with optimizing hole-transport across AIL/donor interface. More importantly, even though r-GO behaves as a metal with a negligible band gap, which is generally considered to cause a lack of electron-blocking properties at the anode contact in organic devices, excellent contact-selectivity is realized in BHJ-OPVs with SR-GO by simply introducing sulfonic acid unit onto the surface of r-GO.

■ ASSOCIATED CONTENT

Supporting Information

Devices performance based on P3HT:$PC_{61}BM$ BHJ, the thickness of PR-GO and SR-GO AILs measured by atomic force microscopy, the photovoltaic-parameter dependence on light intensity, UPS spectra of AIL/$PC_{61}BM$, and OFET devices for doping test of organic layer adjacent to different AILs. This material is available free of charge via the Internet at http://pubs.acs.org.

■ AUTHOR INFORMATION

Corresponding Authors

*E-mail: nsi12@jbnu.ac.kr.
*E-mail: kimdy@gist.ac.kr.

Notes

The authors declare no competing financial interest.

■ ACKNOWLEDGMENTS

This work was supported by the National Research Foundation of Korea (NRF) grant funded by the Korea government (MSIP) (no. 2013-059210), Pioneer Research Center Program (NRF-2013M3C1A3065528), Basic Science Research Program (2013R1A1A1011880), GSR (GIST Specialized Research) Project through a grant provided by GIST in 2014, and the Heeger Center for Advanced Materials (HCAM). We thank the Korea Basic Science Institute (KBSI) for AFM and XPS measurements.

■ REFERENCES

(1) Yu, G.; Gao, J.; Hummelen, J. C.; Wudl, F.; Heeger, A. J. Polymer Photovoltaic Cells: Enhanced Efficiencies via a Network of Internal Donor-Acceptor Heterojunctions. *Science* **1995**, *270*, 1789−1791.

(2) Park, S. H.; Roy, A.; Beaupré, S.; Cho, S.; Coates, N.; Moon, J. S.; Moses, D.; Leclerc, M.; Lee, K.; Heeger, A. J. Bulk Heterojunction Solar Cells with Internal Quantum Efficiency Approaching 100%. *Nat. Photonics* **2009**, *3*, 297−303.

(3) Venkataraman, D.; Yurt, S.; Venkatraman, B. H.; Gavvalapalli, N. Role of Molecular Architecture in Organic Photovoltaic Cells. *J. Phys. Chem. Lett.* **2010**, *1*, 947−958.

(4) Chou, K. W.; Yan, B.; Li, R.; Li, E. Q.; Zhao, K.; Anjoum, D. H.; Alvarez, S.; Gassaway, R.; Biocca, A.; Thoroddsen, S. T.; Hexemer, A.; Amassian, A. Spin-Cast Bulk Heterojunction Solar Cells: A Dynamical Investigation. *Adv. Mater.* **2013**, *25*, 1923−1929.

(5) Liang, Y.; Xu, Z.; Xia, J.; Tsai, S.-T.; Wu, Y.; Li, G.; Ray, C.; Yu, L. For the Bright Future-Bulk Heterojunction Polymer Solar Cells with Power Conversion Efficiency of 7.4%. *Adv. Mater.* **2010**, *22*, E135.

(6) You, J.; Dou, L.; Yoshimura, K.; Kato, T.; Ohya, K.; Moriarty, T.; Emery, K.; Chen, C.-C.; Gao, J.; Li, G.; Yang, Y. A Polymer Tandem Solar Cell with 10.6% Power Conversion Efficiency. *Nat. Commun.* **2013**, *4*, 1446.

(7) Xiao, Z.; Yuan, Y.; Yang, B.; VanDerslice, J.; Chen, J.; Dyck, O.; Duscher, G.; Huang, J. Universal Formation of Compositionally Graded Bulk Heterojunction for Efficiency Enhancement in Organic Photovoltaics. *Adv. Mater.* **2014**, DOI: 10.1002/adma.201305196.

(8) Ratcliff, E. L.; Zacher, B.; Armstrong, N. R. Selective Interlayers and Contacts in Organic Photovoltaic Cells. *J. Phys. Chem. Lett.* **2011**, *2*, 1337−1350.

(9) Steim, R.; Koglera, F. R.; Brabec, C. J. Interface Materials for Organic Solar Cells. *J. Mater. Chem.* **2010**, *20*, 2499−2512.

(10) Shao, S.; Liu, J.; Bergqvist, J.; Shi, S.; Veit, C.; Würfel, U.; Xie, Z.; Zhang, F. In Situ Formation of MoO_3 in PEDOT:PSS Matrix: A Facile Way to Produce a Smooth and Less Hygroscopic Hole Transport Layer for Highly Stable Polymer Bulk Heterojunction Solar Cells. *Adv. Energy Mater.* **2013**, *3*, 349−355.

(11) Ratcliff, E. L.; Meyer, J.; Steirer, K. X.; Armstrong, N. R.; Olson, D.; Kahn, A. Energy Level Alignment in PCDTBT:$PC_{70}BM$ Solar Cells: Solution Processed NiO_x for Improved Hole Collection and Efficiency. *Org. Electron.* **2012**, *13*, 744−749.

(12) Hains, A. W.; Ramanan, C.; Irwin, M. D.; Liu, J.; Wasielewski, M. R.; Marks, T. J. Designed Bithiophene-Based Interfacial Layer for High-Efficiency Bulk-Heterojunction Organic Photovoltaic Cells. Importance of Interfacial Energy Level Matching. *ACS Appl. Mater. Interfaces* **2010**, *2*, 175−185.

(13) Li, S. S.; Tu, K. H.; Lin, C. C.; Chen, C. W.; Chhowalla, M. Solution-Processable Graphene Oxide as an Efficient Hole Transport Layer in Polymer Solar Cells. *ACS Nano* **2010**, *4*, 3169−3174.

(14) Liu, J.; Xue, Y.; Gao, Y.; Yu, D.; Durstock, M.; Dai, L. Hole and Electron Extraction Layers Based on Graphene Oxide Derivatives for High-Performance Bulk Heterojunction Solar Cells. *Adv. Mater.* **2012**, *24*, 2228−2233.

(15) Lee, B. R.; Kim, J.-W.; Kang, D.; Lee, D. W.; Ko, S.-J.; Lee, H. J.; Lee, C.-L.; Kim, J. Y.; Shin, H. S.; Song, M. H. Highly Efficient Polymer Light-Emitting Diodes Using Graphene Oxide as a Hole Transport Layer. *ACS Nano* **2012**, *6*, 2984−2991.

(16) Yun, J.-M.; Yeo, J.-S.; Kim, J.; Jeong, H.-G.; Kim, D.-Y.; Noh, Y.-J.; Kim, S.-S.; Ku, B.-C.; Na, S.-I. Solution-Processable Reduced Graphene Oxide as a Novel Alternative to PEDOT:PSS Hole Transport Layers for Highly Efficient and Stable Polymer Solar Cells. *Adv. Mater.* **2011**, *23*, 4923−4928.

(17) Yeo, J.-S.; Yun, J.-M.; Jung, Y.-S.; Kim, D.-Y.; Noh, Y.-J.; Kim, S.-S.; Na, S.-I. Sulfonic Acid-Functionalized, Reduced Graphene Oxide as an Advanced Interfacial Material Leading to Donor Polymer-Independent High-Performance Polymer Solar Cells. *J. Mater. Chem. A* **2014**, *2*, 292−298.

(18) Ratcliff, E. L.; Meyer, J.; Steirer, K. X.; Garcia, A.; Berry, J. J.; Ginley, D. S.; Olson, D. C.; Kahn, A.; Armstrong, N. R. Evidence for Near-Surface NiOOH Species in Solution-Processed NiO_x Selective Interlayer Materials: Impact on Energetics and the Performance of Polymer Bulk Heterojunction Photovoltaics. *Chem. Mater.* **2011**, *23*, 4988−5000.

(19) Yeo, J.-S.; Yun, J.-M.; Kim, D.-Y.; Park, S.; Kim, S.-S.; Yoon, M.-H.; Kim, T.-W.; Na, S.-I. Significant Vertical Phase Separation in Solvent-Vapor-Annealed Poly(3,4-ethylenedioxythiophene):Poly-(styrene sulfonate) Composite Films Leading to Better Conductivity and Work Function for High-Performance Indium Tin Oxide-Free Optoelectronics. *ACS Appl. Mater. Interfaces* **2012**, *4*, 2551−2560.

(20) Huang, D. M.; Mauger, S. A.; Friedrich, S.; George, S. J.; Dumitriu-LaGrange, D.; Yoon, S.; Moulé, A. J. The Consequences of Interface Mixing on Organic Photovoltaic Device Characteristics. *Adv. Funct. Mater.* **2011**, *21*, 1657−1665.

(21) Kim, D.-H.; Lim, K.-G.; Park, J. H.; Lee, T.-W. Controlling Surface Enrichment in Polymeric Hole Extraction Layers to Achieve High-Efficiency Organic Photovoltaic Cells. *ChemSusChem* **2012**, *5*, 2053−2057.

(22) Choi, M.-R.; Han, T.-H.; Lim, K.-G.; Woo, S.-H.; Huh, D. H.; Lee, T.-W. Soluble Self-Doped Conducting Polymer Compositions with Tunable Work Function as Hole Injection/Extraction Layers in Organic Optoelectronics. *Angew. Chem., Int. Ed.* **2011**, *50*, 6274−6277.

(23) Han, T.-H.; Choi, M.-R.; Woo, S.-H.; Min, S.-Y.; Lee, C.-L.; Lee, T.-W. Molecularly Controlled Interfacial Layer Strategy Toward Highly Efficient Simple-Structured Organic Light-Emitting Diodes. *Adv. Mater.* **2012**, *24*, 1487−1493.

(24) Lee, T.-W.; Chung, Y. Control of the Surface Composition of a Conducting-Polymer Complex Film to Tune the Work Function. *Adv. Funct. Mater.* **2008**, *18*, 2246−2252.

(25) Liao, S.-H.; Jhuo, H.-J.; Cheng, Y.-S.; Chen, S.-A. Fullerene Derivative-Doped Zinc Oxide Nanofilm as the Cathode of Inverted Polymer Solar Cells with Low-Bandgap Polymer (PTB7-Th) for High Performance. *Adv. Mater.* **2013**, *25*, 4766−4711.

(26) Dreyer, D. R.; Park, S.; Bielawski, C. W.; Ruoff, R. S. The Chemistry of Graphene Oxide. *Chem. Soc. Rev.* **2010**, *39*, 228−240.

(27) Zhao, G.; He, Y.; Li, Y. 6.5% Efficiency of Polymer Solar Cells Based on poly(3-hexylthiophene) and Indene-C60 Bisadduct by Device Optimization. *Adv. Mater.* **2010**, *22*, 4355−4358.
(28) Yeo, J.-S.; Yun, J.-M.; Kim, D.-Y.; Kim, S.-S.; Na, S.-I. Successive Solvent-Treated PEDOT:PSS Electrodes for Flexible ITO-Free Organic Photovoltaics. *Sol. Energy Mater. Sol. Cells* **2013**, *114*, 104−109.
(29) Kirchartz, T.; Gong, W.; Hawks, S. A.; Agostinelli, T.; MacKenzie, R. C. I.; Yang, Y.; Nelson, J. Sensitivity of the Mott−Schottky Analysis in Organic Solar Cells. *J. Phys. Chem. C* **2012**, *116*, 7672−7680.
(30) Fabregat-Santiago, F.; Garcia-Belmonte, G.; Mora-Seróa, I.; Bisquert, J. Characterization of Nanostructured Hybrid and Organic Solar Cells by Impedance Spectroscopy. *Phys. Chem. Chem. Phys.* **2011**, *13*, 9083−9118.
(31) Sharma, A.; Yadav, S.; Kumar, P.; Chaudhuri, S. R.; Ghosh, S. Defect States and Their Energetic Position and Distribution in Organic Molecular Semiconductors. *Appl. Phys. Lett.* **2013**, *102*, 143301.
(32) Trukhanov, V. A.; Bruevich, V. V.; Paraschuk, D. Y. Effect of Doping on Performance of Organic Solar Cells. *Phys. Rev. B* **2010**, *84*, 205318.
(33) Garcia-Belmonte, G.; Munar, A.; Barea, E. M.; Bisquert, J.; Ugarte, I.; Pacios, R. Charge Carrier Mobility and Lifetime of Organic Bulk Heterojunctions Analyzed by Impedance Spectroscopy. *Org. Electron.* **2008**, *9*, 847−851.
(34) Nalwa, K. S.; Kodali, H. K.; Ganapathysubramanian, B.; Chaudhary, S. Dependence of Recombination Mechanisms and Strength on Processing Conditions in Polymer Solar Cells. *Appl. Phys. Lett.* **2011**, *99*, 263301.
(35) Mandoc, M. M.; Veurman, W.; Koster, L. J. A.; Boer, B.; de Blom, P. W. M. Origin of the Reduced Fill Factor and Photocurrent in MDMO-PPV:PCNEPV All-Polymer Solar Cells. *Adv. Funct. Mater.* **2007**, *17*, 2167−2173.
(36) Leong, W. L.; Cowan, S. R.; Heeger, A. J. Differential Resistance Analysis of Charge Carrier Losses in Organic Bulk Heterojunction Solar Cells: Observing the Transition from Bimolecular to Trap-Assisted Recombination and Quantifying the Order of Recombination. *Adv. Energy Mater.* **2011**, *1*, 517−522.
(37) Peisert, H.; Knupfer, M.; Zhang, F.; Petr, A.; Dunsch, L.; Fink, J. Charge transfer and doping at organic/organic interfaces. *Appl. Phys. Lett.* **2003**, *83*, 3930.
(38) Wang, H.; Amsalem, P.; Heimel, G.; Salzmann, I.; Koch, N.; Oehzelt, M. Band-Bending in Organic Semiconductors: the Role of Alkali-Halide Interlayers. *Adv. Mater.* **2014**, *26*, 925−930.
(39) Oehzelt, M.; Koch, N.; Heimel, G. Organic Semiconductor Density of States Controls the Energy Level Alignment at Electrode Interfaces. *Nat. Commun.* **2014**, *5*, 4174.
(40) Seo, J. H.; Yang, R.; Brzezinski, J. Z.; Walker, B.; Bazan, G. C.; Nguyen, T.-Q. Electronic Properties at Gold/Conjugated-Polyelectrolyte Interfaces. *Adv. Mater.* **2009**, *21*, 1006−1011.
(41) Qin, P.; Fang, G.; Cheng, F.; Ke, W.; Lei, H.; Wang, H.; Zhao, Z. Sulfur-Doped Molybdenum Oxide Anode Interface Layer for Organic Solar Cell Application. *ACS Appl. Mater. Interfaces* **2014**, *6*, 2963−2973.